# Human CCR6+Th17 lymphocytes are highly sensitive to radiation-induced senescence and are a potential target for prevention of radiation-induced toxicity

Patricia Zadigue, Alexandre De La Taille, Paul-Henri Romeo, Sabine Le Gouvello, Hoang Quy Nguyen, Yazid Belkacemi, Carl Mann, Françoise Hoffschir, Stéphane Kerbrat, Mathieu Surénaud

# Human CCR6$^{+}$Th17 lymphocytes are highly sensitive to radiation-induced senescence and are a potential target for prevention of radiation-induced toxicity

***Running title:*** *Radiation-induced senescence mechanisms*

Hoang Quy Nguyen [a,b], Yazid Belkacemi [a,b,c], Carl Mann [d], Françoise Hoffschir [e], Stéphane Kerbrat [f], Mathieu Surenaud [g], Patricia Zadigue [a,b], Alexandre de La Taille [a,b,h], Paul-Henri Romeo [i§], Sabine Le Gouvello [b,f,j§]

[a] INSERM U955, Equipe 07, Créteil, 94000, France ;
[b] Université de Paris Est, Faculté de Médecine, Créteil, 94000, France ;
[c] APHP, Hôpitaux Universitaires Henri Mondor, Service d'Oncologie Radiothérapie, Créteil, 94000, France ;
[d] Institut de Biologie Intégrative de la Cellule, CEA, CNRS, Université de Paris-Sud, Université de Paris-Saclay, Gif-sur-Yvette cedex, 91198, France ;
[e] CEA/DRF/IBFJ/iRCM/LRTS/Inserm U967, 92265 Fontenay-aux-Roses Cedex, France ;
[f] INSERM UMR955 Team 04, Créteil, 94000, France;
[g] INSERM UMR955 Team 16, Créteil, 94000, France;
[h] APHP, Hôpitaux Universitaires Henri Mondor, Service d'Urologie, Créteil, 94000, France;
[i] CEA/DRF/IBFJ/iRCM/LRTS, 92265 Fontenay-aux-Roses Cedex, France; Inserm U967, Fontenay-aux-Roses cedex, 92265, France; Université de Paris-Diderot, Paris 7, France; Université Paris-Sud, Paris 11, France; Université de Paris-Saclay ; Equipe labellisée Ligue contre le Cancer, France ;
[j] APHP, Hôpital H. Mondor – A. Chenevier, Département de Biologie et Pathologie, Créteil, 94000, France ;

~~*HQ.N. and Y.B. contributed equally to this work as first authors.~~ §PH.R and S.LG share senior authorship. YB. and S.LG were both program directors of HQ.N PhD Thesis.

Corresponding author: Pr Yazid Belkacemi, Radiation Oncology Department & the Henri Mondor Breast Center, University Hospital of Henri Mondor. 51 Av. Mal de Lattre de Tassigny, 94000, Créteil, France. yazid.belkacemi@aphp.fr. Phone: 0033 1 49 814 522; Fax: 00 33 1 45 178 114.

**Conflict of interest: none**

**Acknowledgements**

H.Q.N. was funded by grants from the INCa (PROUST Project), the Ministry of Education and Training (MOET, Vietnam) and the Association for Research and Training in Oncology-Radiotherapy (AREFOR).

C.M. was funded by the ANR-17- 0008-02 and the CEA Radiobiology Program.

The authors wish to thank Adeline Henry, Aurélie Guguin, Odile Ruckebusch from the Flow Cytometry Platform of IMRB/Inserm U955, Créteil, Xavier Decrouy from the Microscope Platform of IMRB/Inserm U955, Créteil for cell sorting, and their technical help and skill.

## Summary

This study demonstrates the high sensitivity of mucosa-homing CCR6$^{+}$Th17 lymphocytes to irradiation (IR)-induced senescence. This senescence is associated with expression of the rare histone variant H2A.J and secretion of IL-8 and VEGF-A. Pharmacological targeting of ROS or MAPKs and/or mTOR signaling pathways prevented this IR-mediated senescence. Altogether, these results suggest potential deleterious effects of irradiated CCR6$^{+}$Th17 lymphocytes during radiotherapy and how these deleterious effects may be prevented.

## Abstract

### Purpose

To study the sensitivity of different peripheral $CD4^+$ T-lymphocyte subsets to IR and identify potential targets for the prevention and/or treatment of radiation-induced toxicity.

### Methods and Materials

This study was performed on peripheral blood mononuclear cells (PBMCs) or sorted peripheral memory lymphocytes of $CCR6^+$ mucosa-homing Th17/$CCR6^{neg}$Th and regulatory T (Treg) subtypes of healthy volunteers. Cells were irradiated with a 2Gy +/- pharmacological inhibitors of different signaling pathways. Senescence of irradiated cells was assessed by resistance to apoptosis and determination of various senescence-associated biomarkers (senescence associated β-galactosidase (SA-β-Gal) activity, $p16^{Ink4a}$-, $p21^{Cdkn1a}$-, γH2A.X-, H2A.J expression). Cytokine production was measured in supernatants of irradiated cells by Luminex technology.

### Results

Not all $CD4^+$ memory T lymphocyte subsets were equally radiosensitive. High sensitivity of $CCR6^+$Th17 lymphocytes to IR-induced senescence was shown by expression of the histone variant H2A.J, higher SA-β-Gal activity and upregulation of $p16^{Ink4a}$ and $p21^{Cdkn1a}$ expression. Lower Annexin V staining and cleaved caspase-3, and higher expression of anti-apoptotic genes Bcl-2 and Bcl-xL LF showed that $CCR6^+$Th17 lymphocytes were more resistant to IR-induced apoptosis than $CCR6^{neg}$ memory Th and Treg lymphocytes. After a 2 Gy IR, both $CCR6^+$Th17 and $CCR6^{neg}$ cells acquired a moderate senescence-associated secretory phenotype (SASP) but only $CCR6^+$Th17 cells secreted IL-8 and VEGF-A. Pharmacological targeting of ROS, MAPKs, and mTOR signaling pathways prevented the expression of senescent markers and IL-8 and VEGF-A expression by $CCR6^+$Th17 cells after IR.

### Conclusion

This study suggests that IR induces senescence of $CCR6^+$Th17 lymphocytes associated with secretion of IL-8 and VEGF-A that may be detrimental to the irradiated tissue. ROS-MAPKs signaling pathways are candidate targets to prevent this $CCR6^+$Th17-dependent radiation-induced potential toxicity. Finally, the ratio of circulating $H2A.J^+$ senescent $CCR6^+$Th17/$CD4^+$ T lymphocytes may be a candidate marker of individual intrinsic radiosensitivity.

## INTRODUCTION

Healthy tissue damage is a limiting factor for radiation therapy. The identification of the radiosensitive patients with predictive assays is needed to tailor radiotherapy plans. Individual radiosensitivity was correlated with resistance of peripheral $CD4^+$ and $CD8^+$ T-cell to IR-induced apoptosis (1–4). Whether the resistance to IR-induced apoptosis of different $CD4^+$ T-lymphocyte subsets contribute to radiation-induced toxicity process has never been investigated.

$CD4^+$ T lymphocytes differentiate into diverse subsets (T helper (Th): Th1, Th2, Th17, *etc*… and regulatory T cell (Treg)) depending on T cell receptor (TCR) activation and the appropriate cytokine microenvironments. These subsets differ by their distinct master transcription factors, the cytokines they produce, and ultimately their functions against invading pathogens or in mediating tolerance (5). The chemokine receptor CCR6 was identified as the main surface marker characterizing the Th17 lineage (6), and regulating the recruitment of both Th17 and Treg cells into inflammatory tissues (7,8). Interestingly, preclinical data demonstrated that the Th17/Th1 lymphocytes ratio was higher in irradiated mouse strains prone to radiation-induced lung fibrosis (9,10). Moreover CCR6 was recently proposed as a predictive biomarker of radiosensitivity (11). Recent data from Veldwijk et al. (12) revealed that $CD4^+$ T lymphocytes are associated with radiotherapy-related adverse late effects of the skin. But the contribution of specific $CD4^+$ antigen-experienced memory T lymphocyte subsets to the pathogenesis of IR-induced non-targeted tissue disabilities remains incompletely understood.

Many studies both *in vitro* and *in vivo* in humans and model organisms support the idea that radiation-accelerated senescence promotes radiation-induced toxicity (13). Cellular senescence (CS) is an irreversible arrest of proliferation triggered by different damaging stimuli, including dysfunctional telomeres, DNA damage, oncogenic mutations, oxidative stress, and IR. Senescent cells are characterized by a combination of different parameters such as β-galactosidase activity, cyclin-dependent kinase inhibitors expression such as $p16^{Ink4a}$ and $p21^{Cdkn1a}$, relative resistance to apoptosis, persistent DNA double-strand breaks (DSBs), a senescence-associated secretory phenotype (SASP) (14,15), and accumulation of the histone variant H2A.J (16). Although "resistance to apoptosis", underlying the above-mentioned radiosensitivity predictive test, could be part of a senescence phenotype, individual sensitivity to IR-induced senescence has never been evaluated as an endpoint to predict radiosensitivity. Therefore, in the present study, we addressed the question of whether $CD4^+CCR6^+$Th17 lymphocytes have a higher sensitivity to IR-dependent apoptosis and/or senescence as compared to $CD4^+CCR6^{neg}$Th and $CCR6^{+\text{ or }neg}$Treg lymphocytes.

## MATERIALS and METHODS

### Cells

Approval for these studies was obtained from the Institutional Review Boards. Written informed consent was obtained from healthy donors according to local institutional guidelines and after approval by the local Ethical Committee in accordance with the Declaration of Helsinki. Peripheral blood mononuclear cells (PBMCs) were separated by Ficoll centrifugation ( UNI-SEPmaxi Tubes (Novamed, Jerusalem, Israel) of healthy donor cytaphereses from the French Blood Bank (EFS, Créteil) .Thirty two individual healthy donors were studied for all experiments shown in this manuscript. As indicated in figure legends, biological replicates were performed for each experimental assay. $CD4^+$ T cells were enriched from PBMCs by negative selection (untouched $CD4^+$ T cell isolation kit, Miltenyi Biotec, Bergisch Gladbach, Germany). $CD4^+CD45RO^+CD127^{neg}CD25^{high}$Treg lymphocytes, $CD4^+$ $CD45RO^+CD127^+CD25^{low}CCR6^+$Th17 lymphocytes and $CD4^+CD45RO^+CD127^+$ $CD25^{low}CCR6^{neg}$Th lymphocytes were further purified (purity ≥99%) by using a fluorescence-activated cell sorter (Influx; BD Biosciences), after labeling with CD127 PE (R34.34), CD45RO ECD (UCHL1, Beckman Coulter, Villepinte, France), CD196 (CCR6) BV 421 or PE-Cy7 (11A9), CD25 APC (2A3, BD Biosciences, Le Pont de Claix, France), CD45RO FITC (UCHL1, Miltenyi Biotec), and CD4 APC eFluor 780 (RPA-T4, eBiosciences, San Diego, CA USA) monoclonal antibodies.

### Irradiation

Cells were plated at $10^6$ cells/ml in 96-well U bottom plates (Corning, Acton, MA USA) in RPMI 1640 Medium GlutaMAX™ HEPES 25mM (Thermo Fisher, Waltham, MA USA), 1 mM sodium pyruvate, 1% MEM Non-Essential Amino Acids Solution, 100 U/ml penicillin, 100 µg/ml streptomycin, supplemented with 10% human AB serum. Cells were irradiated *ex-vivo* at a 2Gy single dose, using gamma radiation from a $^{137}$Cs-source (IBL637; Cis-Bio International/Scherring, Saclay, France) with a dose rate of 2.7 Gy/min.

### Flow cytometric analysis of apoptosis

Irradiated lymphocytes were stained with Annexin V-FITC according to the manufacturer's instructions (BD Biosciences Science) in combination with monoclonal antibodies of the above-mentioned panel, and Viobility Fixable Dye (Miltenyi) for dead cell exclusion. Flow cytometry experiment was performed using an LSR Fortessa X20 (BD Biosciences, France), and Flowlogic software version 7.1 (Miltenyi) was used for subsequent analysis.

### Pharmacologic inhibitors treatments

Prior to IR, cells were pretreated (or not) with 10 mM N-Acetyl-L-cysteine (NAC, Sigma Aldrich) for 1.5 hours, 100nM rapamycin (Sigma Aldrich), 3 µM KU60019 (Sigma Aldrich) for

1 hour, 5µM U0126 (Sigma Aldrich), 5µM JNK-IN-8 (Sigma Aldrich), or 10µM SB203580 (Sigma Aldrich) for 30 minutes (30 min).

**RNA isolation and real time quantitative RT-PCR**

Total mRNA isolation and qRT-PCR analysis were performed as published (17). Primer sequences are listed in Table S1. The expression of all the indicated target transcripts was measured by the relative quantification of real-time PCR using a mix of each cDNA sample as a calibrator sample, according to the ΔΔCt method (18).

**Staining for Senescence-associated β-Galactosidase (SA β-Gal), p16$^{Ink4a}$, cleaved caspase-3, H2AX and H2A.J**

Cells were harvested and spread on Superfrost plus slides (Menzel-Glaser, Braunshweig, Germany) at 1x10$^5$ cells/slide. Staining for SA β-Gal activity (Ozyme, Saint-Quentin-en-Yvelines, France) was performed as described (19).

p16$^{Ink4a}$ analysis: cells were fixed by 4% formaldehyde-PBS for 15 min and incubated overnight at 4°C with anti-p16$^{Ink4a}$ (1:250, Abcam, Cambridge, UK) followed by incubation with Alexa-594 conjugated goat anti-rabbit antibody (1:200, Life Technologies, Saint-Aubin, France) for 1 hour. H2A.J analysis: cells were fixed by 3.7% formaldehyde-PBS, and incubated at room temperature for 1 hour with anti-H2A.J (1:750, gift of Carl Mann (16)), followed by a 1 hour incubation with Alexa-594 (1:500, Life Technologies). After washing, cells were mounted with Prolong Gold+DAPI (Life Technologies) and analyzed on microscope (Carl Zeiss, Oberkochen, Germany).

Caspase 3 activation & phosphoH2A.X expression analysis: cells were fixed by 4% formaldehyde-PBS, washed with PBS and deposited onto poly-D-lysine coated slides. After permeabilization and saturation, cells were incubated with primary antibodies (anti-phospho-histone H2A.X mAb (1:400, Merck Millipore, France) or anti-cleaved Caspase-3 mAb (1:200, Cell Signaling, Ozyme, France) for 1 hour, and then with Alexa-488 conjugated goat anti-mouse antibody (1:750, Life Technologies, Saint-Aubin, France) and Alexa-594 (1:1000, Life Technologies) for 1 hour, respectively. After washing, cells were incubated with DAPI (1:1000, Life Technologies), mounted with Prolong Gold Antifade, and analyzed on a Zeiss Axio Imager microscope driven by MetaSystems software (Altlussheim, Germany).

The images were processed with Image J (http://rsbweb.nih.gov/ij/). For each condition, from 8 to 10 distinct fields representative of the whole of the experimental condition analyzed were photographed. A minimum of 100 cells per condition were analyzed. The percentage of cells with positive labeling is expressed relatively to the number of total cells in the field. The counts were made by two manually blinded independent observers. The cutoff criteria of positive labeling for one cell was determined relatively to the fluorescence intensity of control cells for whom the primary antibodies were not added during the I.F. procedure.

### Cytokine secretion assays

Cell cultures supernatants were analyzed by Luminex assay (PROCARTAPLEX, Thermo Fisher Scientific, Waltham, MA USA), according to the manufacturer's instructions.

### Statistics

Statistical tests were performed using Prism version 5.04 (GraphPad, La Jolla, CA, USA) and data are represented as standard error of the mean (SEM). Differences were assessed with the two-tailed Mann-Whitney U-test. $^{\S}$ indicates a statistical difference between 2 sub-populations ($^{\S}$ $p<0.05$, $^{\S\S}$ $p<0.01$), * in comparison to the non-treated condition (* $p<0.05$, ** $p<0.01$), $^{\&}$ in comparison to the treated condition ($^{\&}$ $p<0.05$, $^{\&\&}$ $p<0.01$). The Kruskal-Wallis test (non-parametric test) was used to compare the sections comprising 3 groups of $CD4^+$T-cell sub-populations.

## RESULTS

### Resting $CCR6^+$Th17 lymphocytes are resistant to a 2Gy IR-induced apoptosis.

We first determined the IR-induced apoptosis of different subsets of $CD4^+$T lymphocytes after irradiation of PBMCs at 2Gy by quantification of $AnnexinV^+$ cells 48 hours after IR (**Fig. 1A**). The following $CD4^+$T lymphocyte subsets were studied: $CCR6^+$T effector/memory lymphocytes (henceforth referred to as "$CCR6^+$Th17") or $CCR6^{neg}$T effector/memory lymphocytes (henceforth referred to as "$CCR6^{neg}$Th") among $CD3^+CD4^+CD45RO^+CD25^{neg}CD127^+$T lymphocytes, and $CD3^+CD4^+CD45RO^+$ $CD25^+$ $CD127^{neg}$ (henceforth referred to as "Treg") with CCR6 positive staining or not. $CCR6^+$Th17 were more resistant to IR-induced apoptosis compared to $CCR6^{neg}$Th and to Treg (**Fig. 1A & 1B**). In addition, $CCR6^+$Treg were more sensitive to IR-induced apoptosis compared to $CCR6^{neg}$Treg (**Fig. 1C**). In accordance, $CCR6^+$Th17 showed a lower activation of caspase-3 than $CCR6^{neg}$Th and Treg (**Fig. 1D & 1E**), and a higher expression of anti-apoptotic effectors (Bcl-2, Bcl-xL LF) after 2Gy IR (**Fig. 1F**). No significant differences could be detected for the other pro- and anti-apoptotic genes (data not shown). Altogether, these results show that resting $CCR6^+$Th17 are resistant to a 2Gy IR-induced apoptosis.

### High IR-induced senescence of $CCR6^+$Th17 cells

Cellular senescence is associated with increased resistance to apoptosis. We thus assayed for canonical hallmarks of senescence in irradiated $CD4^+$T lymphocytes: SA-β-gal activity and expression of the cell cycle inhibitors $p16^{Ink4a}$ and $p21^{Cdkn1a}$ (20). IR induced SA-β-gal activity in $CCR6^+$Th17, $CCR6^{neg}$Th and Treg (**Fig. 2A**), but SA-β-gal activity dose-response was significantly higher for $CCR6^+$Th17 compared to $CCR6^{neg}$Th and Treg (**Fig. 2B**). Moreover, $p16^{Ink4a}$ expression was higher in $CCR6^+$Th17 cells after 2Gy IR (**Fig. 2C & 2D**) and after $H_2O_2$

treatment (**Fig. 2E**). Finally, $p21^{Cdkn1a}$ expression significantly increased after 2Gy IR only in $CCR6^{+}$Th17 (**Fig. 2F**).

We then quantified the secretion of SASP factors (21,22) in supernatants of $CCR6^{+}$Th17 and $CCR6^{neg}$Th 48 hours after 2Gy IR. Supernatants of Treg cultures were not tested because the % of IR-induced apoptotic Treg was high (**Fig. 1A & 1B**) and resultant cellular debris could biased Luminex analysis. Mitogenic stimulation with anti-CD3 and anti-CD28 mAbs, which mimics TCR-dependent activation of T-lymphocyte, was used as a positive control. Compared to this TCR-dependent mitogenic activation, irradiation of $CCR6^{+}$Th17 and $CCR6^{neg}$Th resulted in a moderate secretion of SASP factors with no secretion of IL-13, IL-33 and GM-CSF (**Fig.2G & 2H**). Secretion of IL-1α, IL-6, osteopontin, MIP-1α, and MIP-1β were similarly increased after IR and secretion of IL-1β was increased only in $CCR6^{neg}$Th. Interestingly, irradiated $CCR6^{+}$Th17 secreted larger amounts of VEGF-A and IL-8 compared to irradiated $CCR6^{neg}$Th (**Fig. 2G**).
Altogether, these results show that human $CCR6^{+}$Th17 are highly sensitive to IR-induced senescence associated with VEGF-A and IL-8 secretion.

**Irradiation of $CCR6^{+}$Th17 cells is associated with expression of the rare histone variant H2A.J.**

IR exposure generates DNA double-strand breaks (DSBs) which leads to recruitment of the ATM kinase and phosphorylation of the H2AX histone variant on megabase regions of the chromatin surrounding the DSBs. These so-called γH2AX foci can be quantified by immunofluorescence microscopy. Residual γH2AX foci at 24 hours post-IR are hallmarks of persistent DNA damage associated with several types of senescence (22). We thus investigated DSB repair by enumerating γH2AX foci in sorted, resting $CCR6^{+}$Th17, $CCR6^{neg}$Th and Treg lymphocytes at different time points after 2Gy IR. IR-induced γH2AX foci peaked around 15-30 min post-IR in the three T-lymphocyte subsets which showed similar repair kinetics, but the number of γH2AX foci at 30min after 2Gy IR was higher in $CCR6^{+}$Th17 compared to $CCR6^{neg}$Th and Treg. No significant residual γH2AX foci were found at 24 hours in the three T-lymphocyte subsets, although there was a tendency towards slightly higher foci per cell in $CCR6^{+}$Th17 and $CCR6^{neg}$Th lymphocytes relative to non-irradiated controls (**Fig. 3A & 3B**).

As DNA damage can also impact H2A.J expression (16), we next investigated H2A.J expression in 2Gy-irradiated $CCR6^{+}$Th17 and $CCR6^{neg}$Th. H2A.J expression increased 72 hours after a 2Gy IR of $CCR6^{+}$Th17 and $CCR6^{neg}$Th, but this increased expression was higher in $CCR6^{+}$Th17 (**Fig. 3C & 3D**). The specificity of H2A.J detection was verified by the absence of labeling if the H2A.J peptide, specific of BCR epitopes of the anti-H2A.J antibody, was added as a competitor (PC) during the incubation with the anti-H2A.J antibody in the IF procedure. $H_2O_2$-induced oxidative stress similarly increased H2A.J expression in $CCR6^{+}$Th17 and $CCR6^{neg}$Th

lymphocytes (**Fig. 3E**) suggesting a specific regulation of expression of H2A.J during irradiation of CCR6$^{+}$Th17.

**Inhibition of ROS, MAPKs, and mTOR signaling pathways prevents VEGF-A and IL-8 expression independently of H2A.J expression in senescent CCR6$^{+}$Th17.**

IR increases the production of ROS, which can activate MAPKs signaling pathways (23), which in turn regulate mTOR kinase (24) and the SASP (25). SASP expression has also been correlated with H2A.J accumulation in senescent fibroblasts (16). By using pharmacologically selective inhibitors, we studied the potential involvement of ATM and the ROS-MAPKs-mTOR (26,27) signaling pathways in IR-induced senescence of CCR6$^{+}$Th17. CCR6$^{+}$Th17 and CCR6$^{neg}$Th lymphocytes were pretreated with the ATM inhibitor (KU60019), a ROS scavenger NAC, a p38-MAPK inhibitor (SB203580), a JNK-MAPK inhibitor (JNK-IN-8), a MEK1/2 inhibitor (U0126) or a mTOR inhibitor (rapamycin) before a 2Gy IR. Pretreatment with NAC, rapamycin, and the three MAPKinase pathway inhibitors prevented the IR-induced upregulation of p16$^{Ink4a}$ expression and SA-β-Gal activity in both CCR6$^{+}$Th17 and CCR6$^{neg}$Th, whereas pretreatment with the ATM inhibitor did not (**Fig. 4A & 4B**). Conversely, IR-induced H2A.J expression was not prevented by pretreatment with NAC, rapamycin and p38-MAPK inhibitor, whereas pretreatment with the ATM inhibitor or MEK1/2 and JNK inhibitors did prevent its expression (**Fig. 4C**). Finally, whereas IR-induced secretion of both IL-8 and VEGF-A was abolished by pretreatment with NAC, pretreatment with rapamycin or with the three MAP Kinase pathways inhibitors only abolished IR-induced VEGF-A but not IL-8 secretion (**Fig. 4D & 4E**).

Altogether, these results showed that inhibition of the MEK/ERK-JNK signaling pathways was the only condition that blocked all IR-induced senescence hallmarks and VEGF-A secretion of CCR6$^{+}$Th17.

## DISCUSSION

### *IR-induced accelerated senescence in CCR6$^{+}$Th17*

Cellular senescence (CS) is an irreversible arrest of proliferation triggered by different damaging stimuli, including IR. Similarly to IR-induced senescence in fibroblasts, epithelial, endothelial and mesenchymal stem cells (28–31), we found that IR of CCR6$^{+}$Th17 led to senescence as shown by increased expression of SA-β-gal activity, p16$^{Ink4a}$ and p21$^{Cdkn1a}$. Accordingly, we next demonstrated that CCR6$^{+}$Th17 were more resistant to IR-induced apoptosis compared with CCR6$^{neg}$Th and Treg among PBMCs, as well as when sorted corresponding cells were compared (**Fig. 1 & 2**). Additionally, the irradiated CCR6$^{+}$Th17 upregulated anti-apoptotic genes (Bcl-2, Bcl-xL LF) that presumably accounted for this resistance to apoptosis (**Fig. 1D**). These results agree with previous findings that Bcl-2 proteins were increased in senescent fibroblasts (32). In line with this, CD34$^{+}$ hematopoietic stem cells are thought to be more resistant to apoptosis than other hematopoietic cells because of their higher expression of anti-apoptotic proteins (33), and

Muranski et al. showed that Th17 were long-lived by retaining stem cell-like characteristics (34). We noted that CCR6$^{neg}$Treg were more resistant to IR-induced apoptosis compared with CCR6$^{+}$Treg (**Fig. 1C**), although our results showed that Treg were less resistant to IR-induced apoptosis compared to CCR6$^{+}$Th17 and CCR6$^{neg}$Th. In contrast, a previous study demonstrated that Treg were more resistant to apoptosis than CD4$^{+}$T-lymphocyte in the PBMCs (35), but the authors did not investigate these CCR6$^{+}$Th17, CCR6$^{neg}$Th, CCR6$^{+}$Treg, CCR6$^{neg}$Treg T-lymphocyte subsets in their study.

***IR-induced senescence of CCR6$^{+}$Th17 cells is associated with expression of H2A.J despite completion of DDR.***

We found no significant differences in the decay and residual levels of γH2AX foci post-IR in CCR6$^{+}$Th17 compare to CCR6$^{neg}$Th and Treg (**Fig. 3A & 3B**). Similarly, 1Gy IR of quiescent bone marrow cells (30), or 2Gy IR of quiescent young and old haematopoietic stem cells did not yield residual γH2AX foci 24 hours post-IR (30,36). After much higher levels of IR (15Gy) in the presence of an apoptosis inhibitor, an increase in persistent γH2AX foci was observed for the IR-induced senescence of quiescent endothelial cells (37).

Senescent cells are metabolically active and exhibit widespread modifications in protein expression and secretion corresponding to the SASP that may damage neighboring healthy tissues (38). The accumulation of Histone variant H2A.J promotes inflammatory genes expression (16).

In our study, ATM inhibition did not affect p16$^{Ink4a}$ (**Fig. 4A**), SA-β-Gal (**Fig. 4B**), and two SASP factors secretion, VEGF-A and IL-8 (**Fig. 4D & 4E**) after IR of resting (TCR-nonstimulated) CCR6$^{+}$Th17 and CCR6$^{neg}$Th. This contrasts with a previous study showing that senescence of TCR-stimulated CD4$^{+}$ Th lymphocytes was induced by Treg in part via DNA damage and ATM activation (39). Therefore, ATM-dependent signaling pathways are not necessary for senescence induction after IR of resting Th lymphocytes. Moreover, ATM inhibition prevented H2A.J expression in irradiated CCR6$^{+}$Th17 (**Fig. 4C).** Thus, increased H2A.J levels are not required for the expression of the VEGF-A and IL-8 under these conditions in contrast to a role for accumulated H2A.J in the expression of SASP genes during etoposide-induced senescence of fibroblasts (16). This suggests that H2AJ may not be a marker for premature senescence in T cells. Alternatively, H2A.J expression should be evaluated in replicative senescent T cells (in aged patients for instance) as already shown in replicative senescent fibroblasts (16). The striking inhibition of H2A.J accumulation observed after pre-treatment with the ATM inhibitor suggests that ATM is activated after IR of CCR6$^{+}$Th17 despite the apparent absence of residual γH2AX foci 24 hours post-IR (**Fig. 3A & 3B**). ATM can be activated by oxidative stress, but NAC did not inhibit H2A.J expression after IR, and $H_2O_2$-induced increased H2A.J expression was similar in CCR6$^{+}$Th17 and CCR6$^{neg}$Th (**Fig. 3E**). This

suggests a specific regulation of H2A.J expression during irradiation of CCR6$^{+}$Th17, presumably through a transient activation of ATM by DNA DSBs (**Fig. 4C**), independently of ROS.

Inhibition of the MEK-ERK pathway also blocked H2A.J expression. Since the MEK-ERK pathway is known to be activated in an ATM-dependent fashion in response to DNA damage (40–42), we suggest that ATM-MEK-ERK cascade defines a pathway required for H2A.J expression after IR that might be particularly active in CCR6$^{+}$Th17 compared to other CD4$^{+}$T lymphocytes. In support of this, previous results showed that the MEK1/2-ERK1/2 signaling pathway is critical for proper Th17 differentiation and activation (43–45).

***Signaling pathways of IR-induced senescence***

We found that activation of the p38-MAPK, ERK1/2, JNK and mTOR signaling pathways were required for increased expression of SA-β-Gal, p16$^{Ink4a}$, and VEGF-A (but not IL-8), independently of ATM activity (**Fig. 4**). Remarkably, inhibition of ROS with N-acetyl-cysteine profoundly inhibited all senescence features including IL-8 expression with the exception of H2A.J accumulation (**Fig. 4**). It thus appears that ROS are crucial for IR-induced senescence of the CCR6$^{+}$Th17 and CCR6$^{neg}$Th, presumably by activating downstream signaling pathways including MAPKs and mTOR. It is well-documented that IR can trigger ROS formation and ROS-induced senescence via p38-MAPK and ERK1/2 activation leading to p16$^{Ink4a}$ expression (46,47). Inhibition of VEGF-A expression by individual inhibition of ROS, MAPKs, or mTOR suggests that these represent a single interdependent signaling pathway which might be related to the critical role of MEK-ERK shown in Th17 (43–45). The ROS-MAPKs-mTOR pathway can potentially activate VEGF-A expression via HIF-1α (48,49). In contrast, IL-8 secretion was blocked only by NAC, so we suggest that ROS activate at least two independent downstream signaling pathways in CCR6$^{+}$Th17 that contribute to IL-8 expression (**Fig. 4E**).

## CONCLUSION

To our knowledge, this is the first study to demonstrate high sensitivity of CCR6$^{+}$Th17 to IR-induced senescence. We show that IR-induced senescence of CCR6$^{+}$Th17 promotes IL-8 and VEGF-A secretion that may contribute to IR-induced normal tissue damage and even facilitate tumor recurrence and metastasis after radiotherapy. IR-induced senescence in CCR6$^{+}$Th17 lymphocytes was largely independent of ATM activity, but highly dependent on ROS generation and MEKs/ERK/JNK pathways as seen by the strong suppressing action of N-acetyl-cysteine and MEKs inhibitors. Our data are encouraging for further research using CD4$^{+}$ T lymphocytes subtypes as potential intrinsic radiosensitivity hallmarks, and Bcl-2 /Bcl-xl and the MAPKs pathways as target for senolytic drugs to overcome late inflammation after radiotherapy.

## REFERENCES

1. Ozsahin M, Crompton NEA, Gourgou S, Kramar A, Li L, Shi Y, et al. CD4 and CD8 T-lymphocyte apoptosis can predict radiation-induced late toxicity: a prospective study in 399 patients. Clin Cancer Res Off J Am Assoc Cancer Res. 2005 Oct 15;11(20):7426–33.

2. Azria D, Betz M, Bourgier C, Jeanneret Sozzi W, Ozsahin M. Identifying patients at risk for late radiation-induced toxicity. Crit Rev Oncol Hematol. 2012 Dec;84 Suppl 1:e35-41.

3. Azria D, Riou O, Castan F, Nguyen TD, Peignaux K, Lemanski C, et al. Radiation-induced CD8 T-lymphocyte Apoptosis as a Predictor of Breast Fibrosis After Radiotherapy: Results of the Prospective Multicenter French Trial. EBioMedicine. 2015 Oct 25;2(12):1965–73.

4. COPERNIC project investigators, Granzotto A, Benadjaoud MA, Vogin G, Devic C, Ferlazzo ML, et al. Influence of Nucleoshuttling of the ATM Protein in the Healthy Tissues Response to Radiation Therapy: Toward a Molecular Classification of Human Radiosensitivity. Int J Radiat Oncol Biol Phys. 2016 Mar 1;94(3):450–60.

5. Stockinger B, Omenetti S. The dichotomous nature of T helper 17 cells. Nat Rev Immunol. 2017 Sep;17(9):535–44.

6. Wacleche VS, Landay A, Routy J-P, Ancuta P. The Th17 Lineage: From Barrier Surfaces Homeostasis to Autoimmunity, Cancer, and HIV-1 Pathogenesis. Viruses. 2017 19;9(10).

7. Yamazaki T, Yang XO, Chung Y, Fukunaga A, Nurieva R, Pappu B, et al. CCR6 regulates the migration of inflammatory and regulatory T cells. J Immunol Baltim Md 1950. 2008 Dec 15;181(12):8391–401.

8. Ranasinghe R, Eri R. Modulation of the CCR6-CCL20 Axis: A Potential Therapeutic Target in Inflammation and Cancer. Med Kaunas Lith. 2018 Nov 16;54(5).

9. Paun A, Kunwar A, Haston CK. Acute adaptive immune response correlates with late radiation-induced pulmonary fibrosis in mice. Radiat Oncol Lond Engl. 2015 Feb 20;10:45.

10. Paun A, Bergeron M-E, Haston CK. The Th1/Th17 balance dictates the fibrosis response in murine radiation-induced lung disease. Sci Rep. 2017 Sep 14;7(1):11586.

11. Chang H, Wei J, Tao Y, Ding P, Xia Y, Gao Y, et al. CCR6 Is a Predicting Biomarker of Radiosensitivity and Potential Target of Radiosensitization in Rectal Cancer. Cancer Res Treat Off J Korean Cancer Assoc. 2018 Oct;50(4):1203–13.

12. Veldwijk MR, Seibold P, Botma A, Helmbold I, Sperk E, Giordano FA, et al. Association of CD4+ Radiation-Induced Lymphocyte Apoptosis with Fibrosis and Telangiectasia after Radiotherapy in 272 Breast Cancer Patients with >10-Year Follow-up. Clin Cancer Res Off J Am Assoc Cancer Res. 2019 Jan 15;25(2):562–72.

13. Nguyen HQ, To NH, Zadigue P, Kerbrat S, De La Taille A, Le Gouvello S, et al. Ionizing radiation-induced cellular senescence promotes tissue fibrosis after radiotherapy. A review. Crit Rev Oncol Hematol. 2018 Sep;129:13–26.

14. Campisi J. Cellular Senescence and Lung Function during Aging. Yin and Yang. Ann Am Thorac Soc. 2016 Dec;13(Suppl 5):S402–6.

15. Hernandez-Segura A, Nehme J, Demaria M. Hallmarks of Cellular Senescence. Trends Cell Biol. 2018 Jun 1;28(6):436–53.

16. Contrepois K, Coudereau C, Benayoun BA, Schuler N, Roux P-F, Bischof O, et al. Histone variant H2A.J accumulates in senescent cells and promotes inflammatory gene expression. Nat Commun [Internet]. 2017 May 10 [cited 2018 Jul 6];8. Available from: https://www.ncbi.nlm.nih.gov/pmc/articles/PMC5436145/

17. Guillot-Delost M, Le Gouvello S, Mesel-Lemoine M, Cheraï M, Baillou C, Simon A, et al. Human CD90 identifies Th17/Tc17 T cell subsets that are depleted in HIV-infected patients. J Immunol Baltim Md 1950. 2012 Feb 1;188(3):981–91.

18. Gibson UE, Heid CA, Williams PM. A novel method for real time quantitative RT-PCR. Genome Res. 1996 Oct;6(10):995–1001.

19. Dimri GP, Lee X, Basile G, Acosta M, Scott G, Roskelley C, et al. A biomarker that identifies senescent human cells in culture and in aging skin in vivo. Proc Natl Acad Sci. 1995 Sep 26;92(20):9363–7.

20. Kuilman T, Michaloglou C, Mooi WJ, Peeper DS. The essence of senescence. Genes Dev. 2010 Nov 15;24(22):2463–79.

21. Coppé J-P, Kauser K, Campisi J, Beauséjour CM. Secretion of vascular endothelial growth factor by primary human fibroblasts at senescence. J Biol Chem. 2006 Oct 6;281(40):29568–74.

22. Rodier F, Coppé J-P, Patil CK, Hoeijmakers WAM, Muñoz DP, Raza SR, et al. Persistent DNA damage signaling triggers senescence-associated inflammatory cytokine secretion. Nat Cell Biol. 2009 Aug;11(8):973–9.

23. Werner E, Wang H, Doetsch PW. Opposite Roles for p38MAPK-Driven Responses and Reactive Oxygen Species in the Persistence and Resolution of Radiation-Induced Genomic Instability. PLoS ONE [Internet]. 2014 Oct 1 [cited 2019 May 22];9(10). Available from: https://www.ncbi.nlm.nih.gov/pmc/articles/PMC4182705/

24. Herranz N, Gallage S, Mellone M, Wuestefeld T, Klotz S, Hanley CJ, et al. mTOR regulates MAPKAPK2 translation to control the senescence-associated secretory phenotype. Nat Cell Biol. 2015 Sep;17(9):1205–17.

25. Freund A, Patil CK, Campisi J. p38MAPK is a novel DNA damage response-independent regulator of the senescence-associated secretory phenotype. EMBO J. 2011 Apr 20;30(8):1536–48.

26. Zhu K-Q, Zhang S-J. Involvement of ATM/ATR-p38 MAPK cascade in MNNG induced G1-S arrest. World J Gastroenterol. 2003 Sep 15;9(9):2073–7.

27. Alexander A, Cai S-L, Kim J, Nanez A, Sahin M, MacLean KH, et al. ATM signals to TSC2 in the cytoplasm to regulate mTORC1 in response to ROS. Proc Natl Acad Sci. 2010 Mar 2;107(9):4153–8.

28. Alessio N, Del Gaudio S, Capasso S, Di Bernardo G, Cappabianca S, Cipollaro M, et al. Low dose radiation induced senescence of human mesenchymal stromal cells and impaired the autophagy process. Oncotarget. 2014 Dec 16;6(10):8155–66.

29. Minieri V, Saviozzi S, Gambarotta G, Lo Iacono M, Accomasso L, Cibrario Rocchietti E, et al. Persistent DNA damage-induced premature senescence alters the functional features of human bone marrow mesenchymal stem cells. J Cell Mol Med. 2015 Apr;19(4):734–43.

30. Pustovalova M, Astrelina TA, Grekhova A, Vorobyeva N, Tsvetkova A, Blokhina T, et al. Residual γH2AX foci induced by low dose x-ray radiation in bone marrow mesenchymal stem cells do not cause accelerated senescence in the progeny of irradiated cells. Aging. 2017 Nov 21;9(11):2397–410.

31. Miyake T, Shimada M, Matsumoto Y, Okino A. DNA damage response after ionizing radiation exposure in skin keratinocytes derived from human induced pluripotent stem cells. Int J Radiat Oncol • Biol • Phys [Internet]. 2019 May 11 [cited 2019 May 22];0(0). Available from: https://www.redjournal.org/article/S0360-3016(19)30706-0/abstract

32. Yosef R, Pilpel N, Tokarsky-Amiel R, Biran A, Ovadya Y, Cohen S, et al. Directed elimination of senescent cells by inhibition of BCL-W and BCL-XL. Nat Commun. 2016 Apr 6;7:11190.

33. Durdik M, Kosik P, Kruzliakova J, Jakl L, Markova E, Belyaev I. Hematopoietic stem/progenitor cells are less prone to undergo apoptosis than lymphocytes despite similar DNA damage response. Oncotarget. 2017 Mar 22;8(30):48846–53.

34. Muranski P, Borman ZA, Kerkar SP, Klebanoff CA, Ji Y, Sanchez-Perez L, et al. Th17 Cells Are Long Lived and Retain a Stem Cell-like Molecular Signature. Immunity. 2011 Dec 23;35(6):972–85.

35. Winzler C, Fantinato M, Giordan M, Calore E, Basso G, Messina C. CD4+ T regulatory cells are more resistant to DNA damage compared to CD4+ T effector cells as revealed by flow cytometric analysis. Cytometry A. 2011;79A(11):903–11.

36. Flach J, Bakker ST, Mohrin M, Conroy PC, Pietras EM, Reynaud D, et al. Replication stress is a potent driver of functional decline in ageing haematopoietic stem cells. Nature. 2014 Aug 14;512(7513):198–202.

37. Lafargue A, Degorre C, Corre I, Alves-Guerra M-C, Gaugler M-H, Vallette F, et al. Ionizing radiation induces long-term senescence in endothelial cells through mitochondrial respiratory complex II dysfunction and superoxide generation. Free Radic Biol Med. 2017 Jul;108:750–9.

38. Barratt SL, Flower VA, Pauling JD, Millar AB. VEGF (Vascular Endothelial Growth Factor) and Fibrotic Lung Disease. Int J Mol Sci [Internet]. 2018 Apr 24 [cited 2019 Jul 16];19(5). Available from: https://www.ncbi.nlm.nih.gov/pmc/articles/PMC5983653/

39. Liu X, Mo W, Ye J, Li L, Zhang Y, Hsueh EC, et al. Regulatory T cells trigger effector T cell DNA damage and senescence caused by metabolic competition. Nat Commun. 2018 Jan 16;9(1):249.

40. Tang D, Wu D, Hirao A, Lahti JM, Liu L, Mazza B, et al. ERK Activation Mediates Cell Cycle Arrest and Apoptosis after DNA Damage Independently of p53. J Biol Chem. 2002 Apr 12;277(15):12710–7.

41. Golding SE, Rosenberg E, Neill S, Dent P, Povirk LF, Valerie K. Extracellular Signal-Related Kinase Positively Regulates Ataxia Telangiectasia Mutated, Homologous Recombination Repair, and the DNA Damage Response. Cancer Res. 2007 Feb 1;67(3):1046–53.

42. Heo J-I, Oh S-J, Kho Y-J, Kim J-H, Kang H-J, Park S-H, et al. ATM mediates interdependent activation of p53 and ERK through formation of a ternary complex with p-p53 and p-ERK in response to DNA damage. Mol Biol Rep. 2012 Aug;39(8):8007–14.

43. Tan AH-M, Lam K-P. Pharmacologic Inhibition of MEK–ERK Signaling Enhances Th17 Differentiation. J Immunol. 2010 Feb 15;184(4):1849–57.

44. Liu H, Yao S, Dann SM, Qin H, Elson CO, Cong Y. ERK differentially regulates Th17- and Treg-cell development and contributes to the pathogenesis of colitis. Eur J Immunol. 2013;43(7):1716–26.

45. Kerbrat S, Vingert B, Junier M-P, Castellano F, Renault-Mihara F, Dos Reis Tavares S, et al. Absence of the Adaptor Protein PEA-15 Is Associated with Altered Pattern of Th Cytokines Production by Activated CD4+ T Lymphocytes In Vitro, and Defective Red Blood Cell Alloimmune Response In Vivo. PloS One. 2015;10(8):e0136885.

46. Muller M. Cellular senescence: molecular mechanisms, in vivo significance, and redox considerations. Antioxid Redox Signal. 2009 Jan;11(1):59–98.

47. Shao L, Wang Y, Chang J, Luo Y, Meng A, Zhou D. Hematopoietic stem cell senescence and cancer therapy-induced long-term bone marrow injury. Transl Cancer Res. 2013 Oct;2(5):397.

48. Jing Y, Liu L-Z, Jiang Y, Zhu Y, Guo NL, Barnett J, et al. Cadmium Increases HIF-1 and VEGF Expression through ROS, ERK, and AKT Signaling Pathways and Induces Malignant Transformation of Human Bronchial Epithelial Cells. Toxicol Sci. 2012 Jan;125(1):10–9.

49. Kim D, Dai J, Park Y-H, Fai LY, Wang L, Pratheeshkumar P, et al. Activation of Epidermal Growth Factor Receptor/p38/Hypoxia-inducible Factor-1α Is Pivotal for

Angiogenesis and Tumorigenesis of Malignantly Transformed Cells Induced by Hexavalent Chromium. J Biol Chem. 2016 29;291(31):16271–81.

## FIGURE LEGENDS

**Figure 1: Resistance to IR-induced apoptosis of CCR6$^{+}$Th17 lymphocytes**

(A) Representative flow cytometric gating strategy illustrating lymphocyte CD4$^{+}$T-lymphocyte subsets in PBMCs. Cells treated with 2Gy-IR and analyzed by flow cytometry 48 hours post-IR.

(B-C) %Apoptosis (%Apoptosis 2Gy – %Apoptosis 0Gy) at 48 hours within CCR6$^{+}$Th17/ CCR6$^{neg}$Th/Treg (B), and within CCR6$^{+}$Treg/CCR6$^{neg}$Treg (C). n=6, mean +/- SEM.

(D-E) Epifluorescence microscopy was applied to assess cleaved caspase-3 in CCR6$^{+}$Th17/CCR6$^{neg}$Th/Treg at 24 hours after 2 Gy IR. Image acquisition was performed with a Zeiss Axio Imager microscope driven by MetaSystems software. At least 120 cells are counted in one experiment. n=4, mean +/- SEM.

(F) qRT-PCR data showing expression of anti-apoptotic genes Bcl2, Bcl-xL LF.

**Figure 2: IR-induced senescence in CCR6$^{+}$Th17 lymphocytes**

(A) Representative images of SA-β-Gal staining of CCR6$^{+}$Th17/CCR6$^{neg}$Th17/Treg at 48 hours after 2 Gy IR. Senescent cells are blue after SA-β-Gal cytoplasmic staining.

(B) % SA-β-Gal positive cells. 200-800 cells per experimental condition were counted. n=4, mean +/- SEM.

(C) Representative images of p16$^{Ink4a}$ immunofluorescence in CCR6$^{+}$Th17/ CCR6$^{neg}$Th/Treg at 24 hours after 2 Gy IR.

(D-E) % p16$^{Ink4a}$ positive cells. 150–500 cells per condition were counted. n=4, mean +/- SEM. (D) Cells were treated with 2 Gy IR. (E) Cells were treated with $H_2O_2$ at the indicated concentrations for 72 hours.

(F) qRT-PCR showing expression of p21$^{Cdkn1a}$ in CCR6$^{+}$Th17/CCR6$^{neg}$Th/Treg. n=5, mean +/- SEM.

(G-H) Comparative cytokine production of CCR6$^{+}$Th17/CCR6$^{neg}$Th at 72 hours after 2 Gy IR (n=7). (G) plate-bound anti-CD3ε (5µg/mL) antibody and soluble anti-CD28 (2µg/mL) antibody

were used as a positive control (n=4). Selected cytokine levels are shown as the fold change over the non-irradiated conditions.

**Figure 3: IR-induced senescence of CCR6$^{+}$Th17 lymphocytes is associated with expression of H2A.J despite completion of the DDR**

(A) Immunofluorescence of γH2AX foci in CCR6$^{+}$Th17/CCR6$^{neg}$Th/Treg lymphocytes at 0, 15, 30 min, and 24 hours after 2 Gy IR.

(B) Quantification of γH2AX foci at 0, 15, 30, 45 min, 1, 6 and 24 hours after 2 Gy IR. At least 120 cells per experimental condition were counted in each experiment. n=4, mean +/- SEM.

(C) Representative images of H2A.J immunofluorescence in CCR6$^{+}$Th17/CCR6$^{neg}$Th at 72 hours after 2 Gy IR with or without peptide competition (PC) of H2A.J antibodies.

(D-E) % H2A.J positive cells. 200–500 cells per experimental condition were counted. n=4, mean +/- SEM. (D) Cells were treated with 2 Gy IR (E) Cells were treated with $H_2O_2$ at the indicated concentrations for 72 hours.

**Figure 4: Effect of pharmacological inhibitors pretreatment on irradiated CCR6$^{+}$Th17/CCR6$^{neg}$Th**

(A-C) % of p16$^{Ink4a}$, β-Gal positive cells, and H2A.J were evaluated. 200–600 cells per experiment condition were counted, mean +/- SEM, n=5 for p16$^{Ink4a}$ & H2A.J (A&C), n=3 for β-Gal (B)

(D-E) Comparative cytokine production of CCR6$^{+}$Th17/CCR6$^{neg}$Th 72 hours after 2 Gy IR. VEGF-A (D) and IL-8 (E) levels are shown as the fold change over the non-irradiated. n=5, mean +/- SEM.

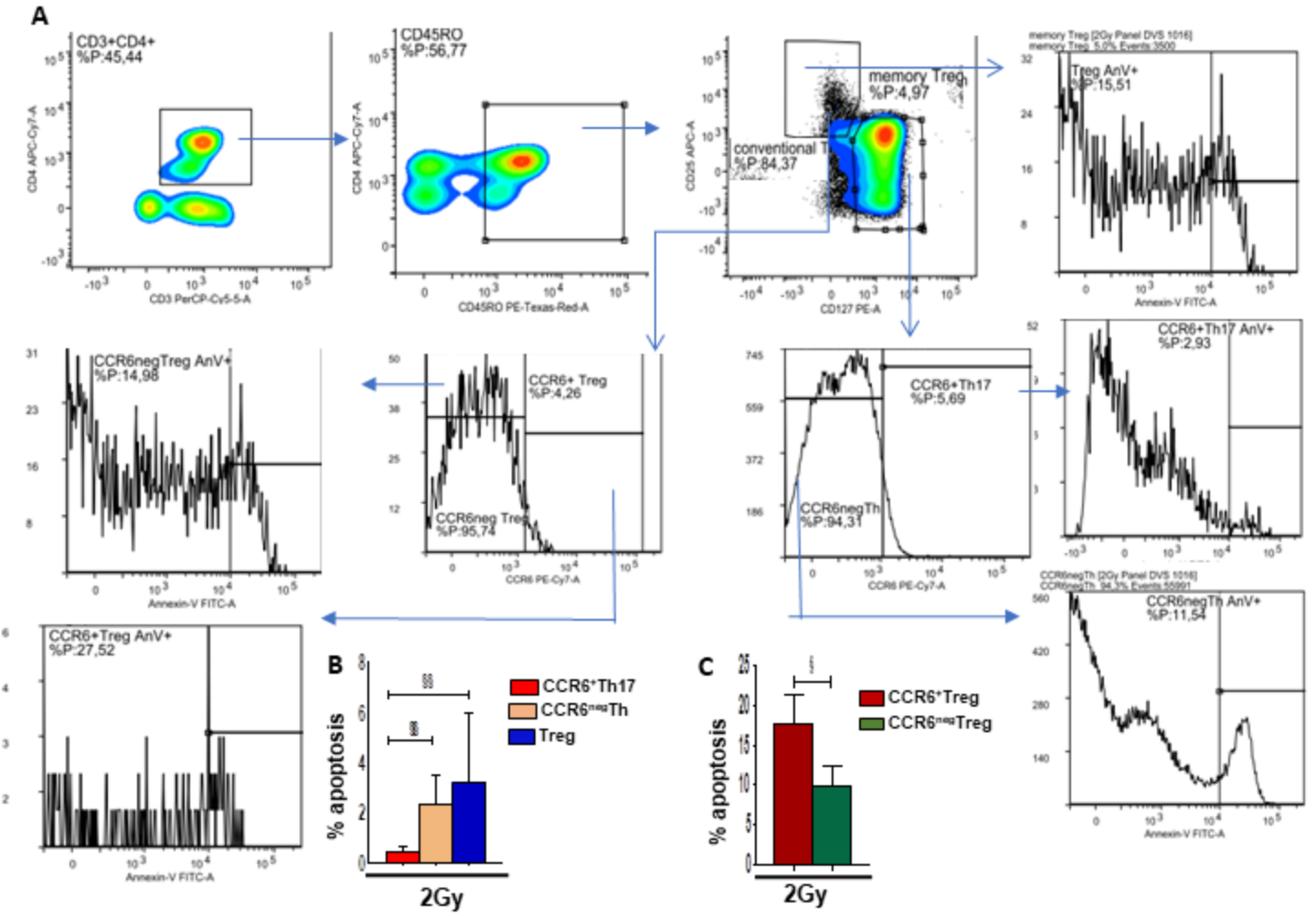
A
CD3+CD4+
%P:45,44
CD45RO
%P:56,77
memory Treg
%P:4,97
conventional T
%P:84,37
Treg AnV+
%P:15,51
CCR6negTreg AnV+
%P:14,98
CCR6+ Treg
%P:4,26
CCR6neg Treg
%P:95,74
CCR6+Th17
%P:5,69
CCR6negTh
%P:94,31
CCR6+Th17 AnV+
%P:2,93
CCR6negTh AnV+
%P:11,54
CCR6+Treg AnV+
%P:27,52
B
% apoptosis
CCR6+Th17
CCR6negTh
Treg
2Gy
C
% apoptosis
CCR6+Treg
CCR6negTreg
2Gy

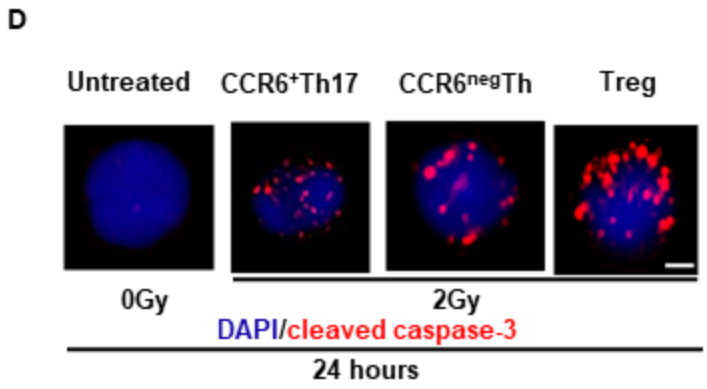
D
Untreated
CCR6+Th17
CCR6negTh
Treg
0Gy
2Gy
DAPI/cleaved caspase-3
24 hours

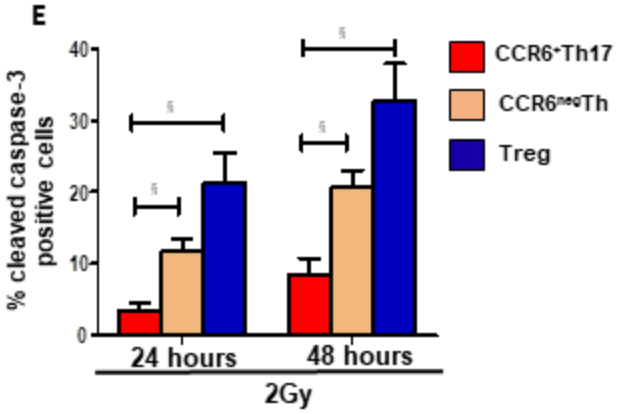
E
% cleaved caspase-3 positive cells
CCR6+Th17
CCR6negTh
Treg
24 hours
48 hours
2Gy

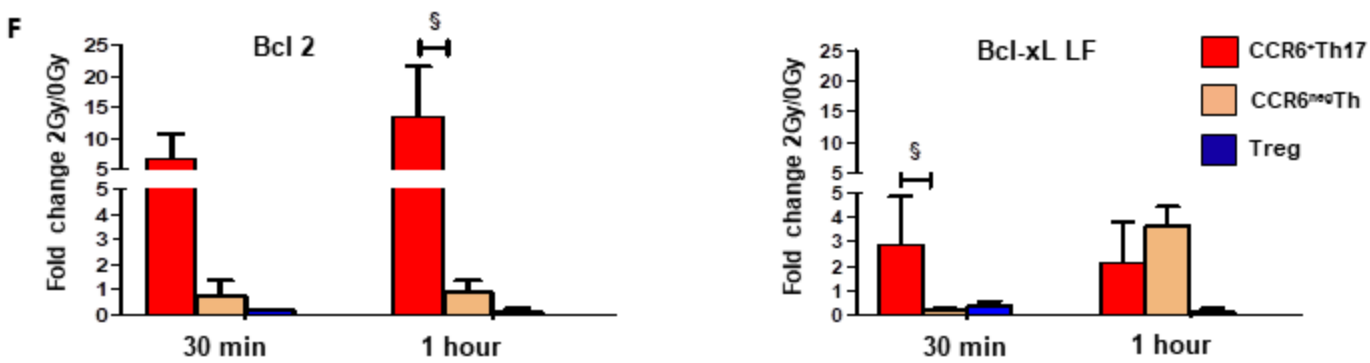
F
Bcl 2
Fold change 2Gy/0Gy
30 min
1 hour
Bcl-xL LF
CCR6+Th17
CCR6negTh
Treg

**Figure 1**

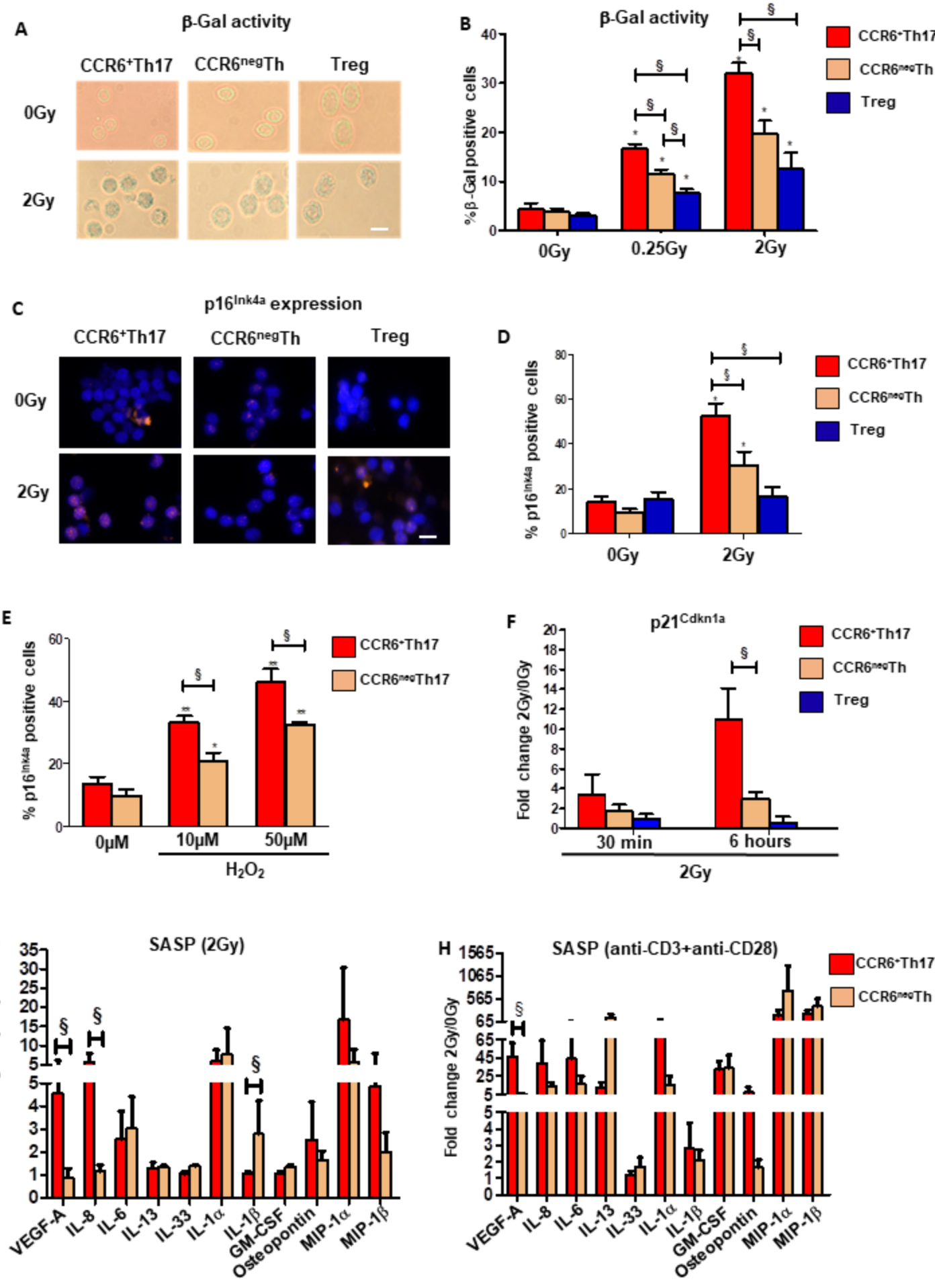
A
β-Gal activity
CCR6+Th17
CCR6negTh
Treg
0Gy
2Gy
B
β-Gal activity
%β-Gal positive cells
0Gy
0.25Gy
2Gy
CCR6+Th17
CCR6negTh
Treg
C
p16Ink4a expression
CCR6+Th17
CCR6negTh
Treg
0Gy
2Gy
D
% p16Ink4a positive cells
0Gy
2Gy
CCR6+Th17
CCR6negTh
Treg
E
% p16Ink4a positive cells
0μM
10μM
50μM
H2O2
CCR6+Th17
CCR6negTh17
F
p21Cdkn1a
Fold change 2Gy/0Gy
30 min
6 hours
2Gy
CCR6+Th17
CCR6negTh
Treg
G
SASP (2Gy)
Fold change 2Gy/0Gy
VEGF-A
IL-8
IL-6
IL-13
IL-33
IL-1α
IL-1β
GM-CSF
Osteopontin
MIP-1α
MIP-1β
H
SASP (anti-CD3+anti-CD28)
Fold change 2Gy/0Gy
VEGF-A
IL-8
IL-6
IL-13
IL-33
IL-1α
IL-1β
GM-CSF
Osteopontin
MIP-1α
MIP-1β
CCR6+Th17
CCR6negTh

**Figure 2**

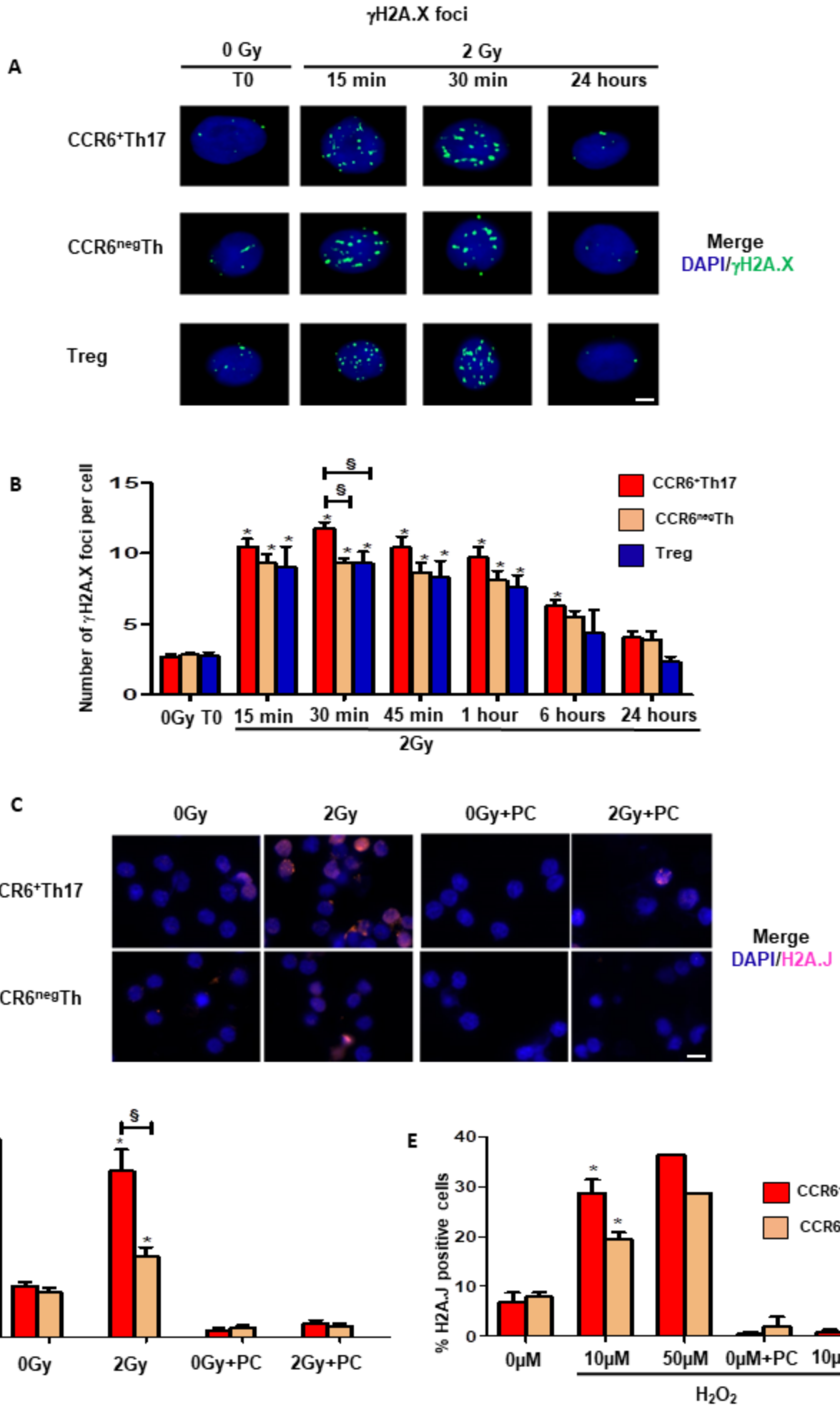
γH2A.X foci
A
0 Gy
2 Gy
T0
15 min
30 min
24 hours
CCR6+Th17
CCR6negTh
Treg
Merge
DAPI/γH2A.X
B
Number of γH2A.X foci per cell
CCR6+Th17
CCR6negTh
Treg
0Gy T0
15 min
30 min
45 min
1 hour
6 hours
24 hours
2Gy
C
0Gy
2Gy
0Gy+PC
2Gy+PC
CCR6+Th17
CCR6negTh
Merge
DAPI/H2A.J
D
% H2A.J positive cells
0Gy
2Gy
0Gy+PC
2Gy+PC
E
% H2A.J positive cells
CCR6+Th17
CCR6negTh
0μM
10μM
50μM
0μM+PC
10μM+ PC
H2O2

Figure 3

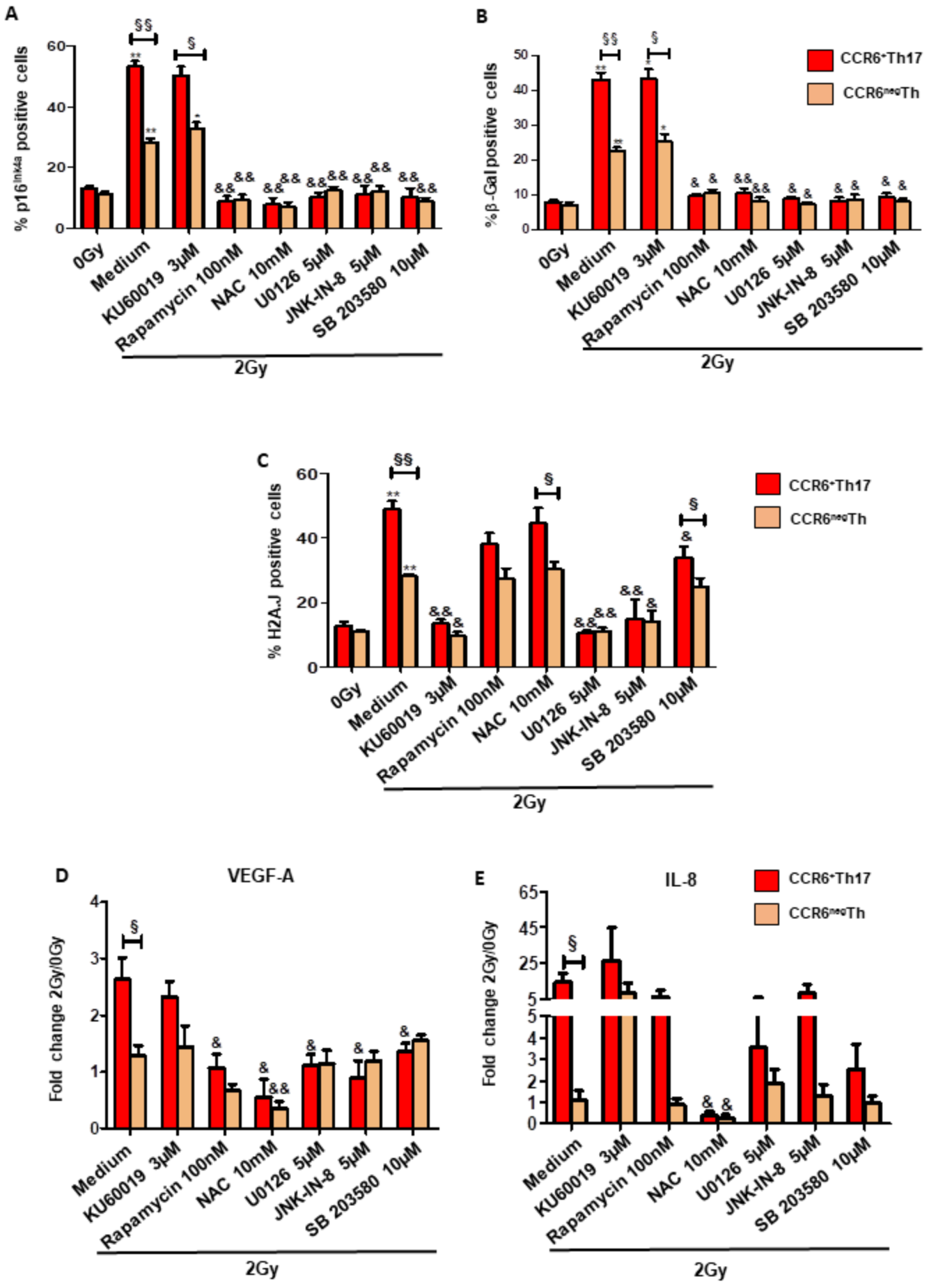
A
% p16INK4a positive cells
60
40
20
0
§§
§
**
**
*
*
&&
0Gy
Medium
KU60019 3µM
Rapamycin 100nM
NAC 10mM
U0126 5µM
JNK-IN-8 5µM
SB 203580 10µM
2Gy
B
% β-Gal positive cells
50
40
30
20
10
0
CCR6+Th17
CCR6negTh
&
&&
C
% H2A.J positive cells
60
40
20
0
D
VEGF-A
Fold change 2Gy/0Gy
4
3
2
1
0
E
IL-8
Fold change 2Gy/0Gy
65
45
25
5
4
3
2
1
0

**Figure 4**